J Solid State Electrochem (2011) 15:2185–2197
DOI 10.1007/s10008-011-1402-z

ORIGINAL PAPER

Electrocatalysis and redox behavior of Pt^{2+} ion in CeO_2 and $Ce_{0.85}Ti_{0.15}O_2$: XPS evidence of participation of lattice oxygen for high activity

Sudhanshu Sharma · Preetam Singh · M. S. Hegde

Received: 1 December 2010 / Revised: 6 April 2011 / Accepted: 9 April 2011 / Published online: 28 April 2011

Abstract Electronic states of CeO_2, $Ce_{1-x}Pt_xO_{2-\delta}$, and $Ce_{1-x-y}Ti_yPt_xO_{2-\delta}$ electrodes have been investigated by X-ray photoelectron spectroscopy as a function of applied potential for oxygen evolution and formic acid and methanol oxidation. Ionically dispersed platinum in $Ce_{1-x}Pt_xO_{2-\delta}$ and $Ce_{1-x-y}Ti_yPt_xO_{2-\delta}$ is active toward these reactions compared with CeO_2 alone. Higher electrocatalytic activity of Pt^{2+} ions in CeO_2 and $Ce_{1-x}Ti_xO_2$ compared with the same amount of Pt^0 in Pt/C is attributed to Pt^{2+} ion interaction with CeO_2 and $Ce_{1-x}Ti_xO_2$ to activate the lattice oxygen of the support oxide. Utilization of this activated lattice oxygen has been demonstrated in terms of high oxygen evolution in acid medium with these catalysts. Further, ionic platinum in CeO_2 and $Ce_{1-x}Ti_xO_2$ does not suffer from CO poisoning effect unlike Pt^0 in Pt/C due to participation of activated lattice oxygen which oxidizes the intermediate CO to CO_2. Hence, higher activity is observed toward formic acid and methanol oxidation compared with same amount of Pt metal in Pt/C.

Keywords Electrocatalysis · Methanol · Formic acid · Oxidation · Electrooxidation · Lattice oxygen · Oxygen activation

S. Sharma (✉)
Chemical Engineering Department, University of California,
Santa Barbara,
Santa Barbara, CA, USA
e-mail: sudhanshu@engineering.ucsb.edu

P. Singh · M. S. Hegde (✉)
Solid State and Structural Chemistry Unit,
Indian Institute of Science,
Bangalore 560012, India
e-mail: mshegde@sscu.iisc.ernet.in

Introduction

Platinum has always been a good choice for several electrochemical reactions because of its stability in both acidic and basic medium and reactivity toward almost all electrochemical reactions. Platinum nanoparticles dispersed over carbon usually denoted by Pt/C are used for electrocatalytic applications for a long time. Platinized platinum, termed as Pt/Pt, is another important catalyst used extensively for several electrocatalytic reactions. Platinum in Pt/C or in Pt/Pt is in the form of metal nanoparticles where Pt is in zero-valent state. These conventional Pt catalysts have been used for catalytic oxidation of formic acid [1–4], methanol [5], H_2O_2 [6], oxygen evolution [7–9], and H_2+O_2 recombination reaction [10, 11]. Formic acid oxidation is of particular importance due to its use in direct formic acid fuel cell, which has various advantages over widely used direct methanol fuel cell, namely faster anode kinetics, lower crossover, and higher open circuit potential [12, 13].

Formic acid electrooxidation on platinum metal surface was believed to follow a "dual" pathway, direct and indirect [14]. One pathway involves fast reaction forming CO_2 directly (dehydrogenation), and the other indirect pathway includes a step in which an inhibiting intermediate CO is formed. Chen et al. have recently demonstrated a third pathway (formate pathway) involving the formation of formate ion also leading to CO_2 [15].

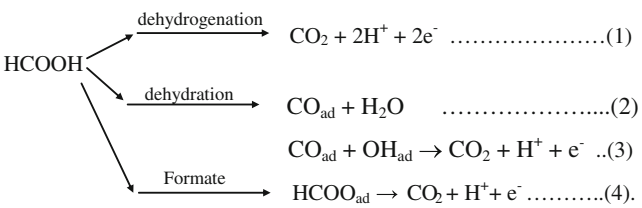

Reactions 2 and 3 lead to CO poisoning effect, and this process is well documented in the literature [14–16]. At lower potentials (~0.2 V), formic acid electrooxidation reaction proceeds via pathway 2, and above 0.2 V, pathway 1 is followed but increase in CO_{ad} coverage leads to the accumulation of CO_{ad}. Due to surface deactivation of platinum via oxide formation above 0.7 V, electrooxidation of HCOOH in forward scan does not occur [1, 17–19]. In the reverse scan once the surface platinum is cleaned after the reduction of platinum oxide, HCOOH oxidation retains. Therefore, due to CO adsorptions/poisoning effect on the platinum metal surface, one would not see high electrooxidation current at lower potential. Various additives such as Fe, Pd or Ru, etc. have been alloyed with platinum to improve the performance for HCOOH oxidation [13, 19–26]. Although unsupported Pd and Pd/C are found to be highly active [1, 17, 27–34], it is unstable under anodic potential [35]. Though Pt/C catalysts are widely employed, due to the limitation of CO adsorption on Pt surface, a number of issues are associated with Pt: (a) Can conventional Pt^0 in any form be replaced to Pt^{2+} ions to increase dispersion and activity? (b) Can an additive like CeO_2 be added to platinum to make use of oxygen storage capacity of CeO_2 to remove CO poisoning effect?

By a novel solution combustion method, $Ce_{1-x}Pt_xO_{2-\delta}$ (x= 0.005–0.02) and $Ce_{0.83}Ti_{0.15}Pt_{0.02}O_{2-\delta}$ were prepared where Pt is found mainly in +2 oxidation state. With these ionic catalysts, 10–15 times higher catalytic activity for CO oxidation was observed due to the ionic dispersion and Pt^{2+}-CeO_2 ionic interaction compared with Pt^0/Al_2O_3 for the same amount of platinum [36]. Pt^{2+} ion in CeO_2 matrix is the active site for CO adsorption, and lattice oxygen is utilized for CO oxidation [37]. Pt^{2+} in CeO_2 and $Ce_{1-x}Ti_xO_2$ is stable in both acid and alkali media, and the Pt ions do not leach out from the material. Therefore, we have explored Pt^{2+} substituted CeO_2 and $Ce_{1-x}Ti_xO_2$ in electrocatalysis for formic acid and methanol oxidation.

X-ray photoelectron spectroscopy (XPS) has earlier been employed [38] ex situ to study the adsorbed oxygen species. There are other studies also which focus on studying the electrochemically treated surfaces using ex situ XPS [39, 40]. Our group adopted this idea recently to study the nature of interaction between Pt^{2+} ion and CeO_2 during electrochemical oxidation and reduction which was found to be electronic [41]. In this report, we have extended the same idea to further investigate the redox and catalytic properties to demonstrate oxygen evolution, formic acid, and methanol oxidation over CeO_2, $Ce_{1-x}Pt_xO_{2-\delta}$, and $Ce_{1-x-y}Ti_yPt_xO_{2-\delta}$ electrodes in acid medium at various electrode potentials. Activity of Pt^{2+} in $Ce_{1-x}Pt_xO_{2-\delta}$ and $Ce_{1-x-y}Ti_yPt_xO_{2-\delta}$ has been compared with Pt/C. We find that there is an interaction between Pt^{2+} ion and support (CeO_2 and $Ce_{1-x}Ti_xO_2$), which has been reflected in terms of higher electrocatalytic activity with $Ce_{1-x}Pt_xO_{2-\delta}$ and $Ce_{1-x-y}Ti_yPt_xO_{2-\delta}$ compared with Pt/C toward formic acid and methanol oxidation. The aim of this work is to investigate the role of lattice oxygen in the electrocatalytic properties, for example, if there is any role of the lattice oxygen in removing the CO poisoning effect during formic acid electrooxidation. We find that indeed lattice oxygen plays a key role in the activity of these doped metal oxides.

Experimental

The catalysts $Ce_{1-x}Pt_xO_{2-\delta}$ (x=0.0025, 0.005, 0.01, 0.015, 0.02) were prepared by solution combustion method [37–42]. In a typical preparation for $Ce_{0.99}Pt_{0.01}O_{2-\delta}$, 5 g of ceric ammonium nitrate, 0.04771 g of H_2PtCl_6, and 2.5877 g of oxalyl dihydrazide (ODH) were dissolved in 15 ml of water in a borosilicate dish of 130-cm^3 capacity. The dish containing the redox solution was introduced into a muffle furnace maintained at 350 °C. Solution boils, froths followed by the combustion with a flame giving the final compound. Similarly, a series of $Ce_{1-x}Pt_xO_{2-\delta}$ (x= 0.0025, 0.005, 0.01, 0.015, 0.02) oxides were prepared by taking the stoichiometric amount of H_2PtCl_6, ODH, and $(NH_4)_2Ce(NO_3)_6$. Pure CeO_2 was prepared by the combustion of the aqueous solution of 5 g of ceric ammonium nitrate and 2.5877 g of ODH. The combustion reactions involved can be written as:

$$10\,(1-x)(NH_4)_2Ce\,(NO_3) + 24(1-x)\,C_2H_6N_4O_2 + 10x\,H_2PtCl_6 \longrightarrow \quad (5)$$

$$10\,Ce_{1-x}Pt_xO_{2-\delta} + 88\,(1-x)\,N_2 + (102-112x)\,H_2O + 48\,(1-x)\,CO_2 + 20x\,HCl$$

$Ce_{0.83}Ti_{0.15}Pt_{0.02}O_{2-\delta}$ was prepared by the combustion of the aqueous solution of $(NH_4)_2Ce(NO_3)_6{\cdot}6H_2O$, $Pt(NH_3)_4(NO_3)_2$, $TiO(NO_3)_2$, and glycine in the mole ratio 0.84:0.01:0.15:2.42. In a typical preparation, $(NH_4)_2Ce(NO_3)_6{\cdot}6H_2O$ (3 g), $Pt(NH_3)_4(NO_3)_2$ (0.0252 g), $TiO(NO_3)_2$ (0.1823 g), and glycine (1.1814 g) were taken. Detailed procedure has been described elsewhere [43]. Characterization of the materials was done by X-ray

diffraction (XRD), XPS, and Brunauer–Emmett–Teller (BET) surface area measurement.

Platinum dispersed over carbon was prepared by impregnating H_2PtCl_6 over carbon followed by reducing with mild reducing agent, formaldehyde; 2.4 mL of 1% H_2PtCl_6 was reduced over 400 mg of carbon powder (pract, S.D. Fine Chemicals) so that 22.4 mg of nanoplatinum metal particles is dispersed per gram of carbon powder.

Electrochemical studies were performed using conventional three electrode system. Working electrode was made by mixing a known amount of catalyst with 30 wt.% of graphitic carbon and 5 wt.% of polyvinylidene difluoride binder followed by depositing a thin layer of this slurry on a graphite paper over a known area. Platinum foil was used as a counter electrode. Saturated calomel electrode was used as a reference electrode. H_2SO_4 (0.5 M) was used as supporting electrolyte.

Electronic states of Ce and Pt ions of electrochemically oxidized and cycled samples were recorded from an X-ray photoelectron spectrometer (Thermo Fisher Scientific Multilab 2000). The electrodes were taken out from the electrochemical cell, dried at 60 °C in an oven, and mounted directly inside the XPS chamber. Since the catalyst was mixed with graphite powder and deposited on graphite paper, there was no observation of charging effect in binding energy of metal ions. Further, due to carbon and binder coating, the electrochemically reduced surface component of Ce_2O_3 from CeO_2 remained in reduced state even on the exposure to air. Binding energies reported here are with respect to C(1s) at 284.5 eV, and they are accurate within ±0.1 eV.

Results and discussion

XRD patterns of $Ce_{1-x}Pt_xO_{2-\delta}$ (x=0.0025, 0.005, 0.01, 0.015, 0.02) are recorded, and they crystallize in the fluorite structure. Crystallite sizes of the $Ce_{0.98}Pt_{0.02}O_{2-\delta}$ powder estimated from the half width of diffraction lines are in the range of 30–40 nm. None of the Pt metal or PtO_x reflections was present in any of the $Ce_{1-x}Pt_xO_{2-\delta}$ compounds indicating substitution of Pt in CeO_2. A detailed study on the Pt^{2+} ion substitution in CeO_2 has been reported earlier [37–42]. XRD pattern of $Ce_{0.83}Ti_{0.15}Pt_{0.02}O_{2-\delta}$ is shown in Fig. 1. In an earlier report from this laboratory, $Ce_{1-x}Ti_xO_2$ (x=0.0–0.5) solid solution formation was reported [43, 44] where a systematic decrease in the lattice parameter was shown confirming the formation of $Ce_{1-x}Ti_xO_2$ solid solutions. Peaks due to TiO_2 in anatase or rutile phase were not detectable up to x=0.4. Moreover, upon 2% of Pt ion substitution by solution combustion, route in $Ce_{0.85}Ti_{0.15}O_2$ and no Pt metal peaks were observed in the powder XRD pattern given in Fig. 1, and thus, compound was represented as

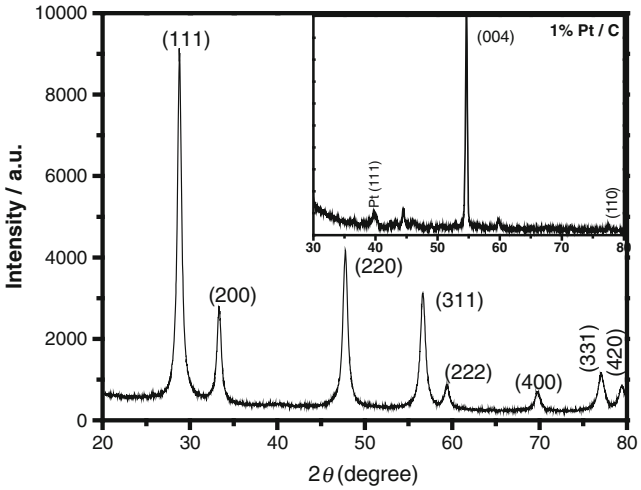

Fig. 1 XRD pattern of $Ce_{0.83}Pt_{0.02}Ti_{0.15}O_{2-\delta}$ and 2% Pt/C (*inset*)

$Ce_{0.83}Ti_{0.15}Pt_{0.02}O_{2-\delta}$. XRD pattern of 2% Pt/C is given in the inset of Fig. 1. Clearly, 2% Pt/C shows a distinct Pt (111) peak at (c) 2θ=39.8° suggesting Pt in the metallic state. By measuring the full width at half maxima particle, size of platinum estimated is ~4 nm. BET surface area of $Ce_{0.98}Pt_{0.02}O_{2-\delta}$ and $Ce_{0.83}Ti_{0.15}Pt_{0.02}O_{2-\delta}$ is 13 and 19 $m^2\ g^{-1}$, respectively.

XPS of Ce(3d) from CeO_2 and Ce_2O_3 show characteristic satellites due to Ce^{4+} and Ce^{3+} ions (see Fig. 2a, b), and they have been discussed in detail by Kotani and Ogasawarab [45]. Linear background subtraction is used for all the Ce(3d) spectra which give an approximate idea. In

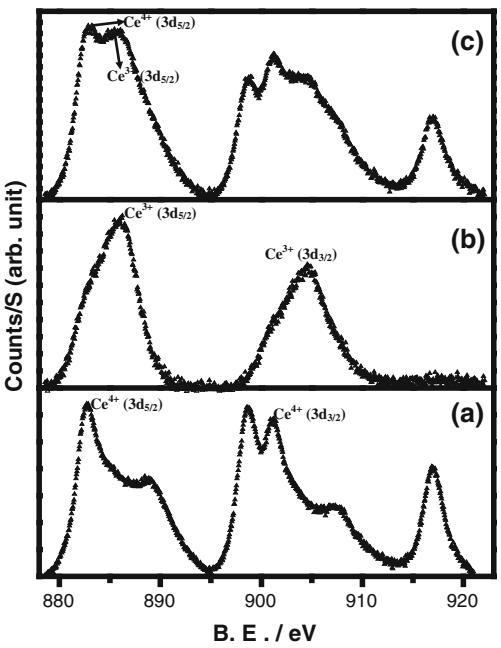

Fig. 2 XPS of Ce(3d) core level spectra in *a* CeO_2, *b* Ce_2O_3, and *c* Ce (3d) core level spectrum obtained by the addition of CeO_2 and Ce_2O_3 in the ratio of 50:50

general, CeO_2 synthesized by combustion/flame method with similar morphology contains small percentage (~5%) of Ce^{3+} state [46]. Even though electrochemically reduced CeO_2 electrode is exposed to air, there was no oxidation of reduced Ce_2O_3 as seen from the complete absence of 917 eV satellite peak (Fig. 2b), a characteristic of CeO_2. This is due to the coating of carbon and binder over oxide. If there is an increase in the Ce^{3+} state due to the reduction of Ce^{4+}, the shape of the spectrum changes. One simple way of estimating the change in the ratio of Ce^{4+}/Ce^{3+} during any oxidation or reduction reaction is to compare the resultant spectrum with the spectrum obtained by the addition of CeO_2 and Ce_2O_3 after normalizing the intensity. For example, the addition of equal percentage of CeO_2 and Ce_2O_3 spectra given in Fig. 2c represents the shape of the mixed valent Ce^{4+} and Ce^{3+} of equal ratio.

X-ray photoelectron spectrum of Pt(4f) region of Pt metal foil, Pt nanoparticles in 2% Pt/C, $Pt(NH_3)_4(NO_3)_2$, and PtO_2 are given in Fig. 3a–d, respectively. $Pt(4f_{7/2})$ peaks are seen at 71.1, 71.4, 72.4, and 75 eV, respectively, for Pt in 0 (for both metal foil and 2% Pt/C), +2 and +4 states. All of these samples except the Pt foil are the powdered material with 5–10 nm of size as particle size is known to affect the binding energy [47]. $Pt(4f_{7/2,5/2})$ core level peaks at 71.4 and 74.8 eV in 2% Pt/C confirm that platinum is present in metallic state.

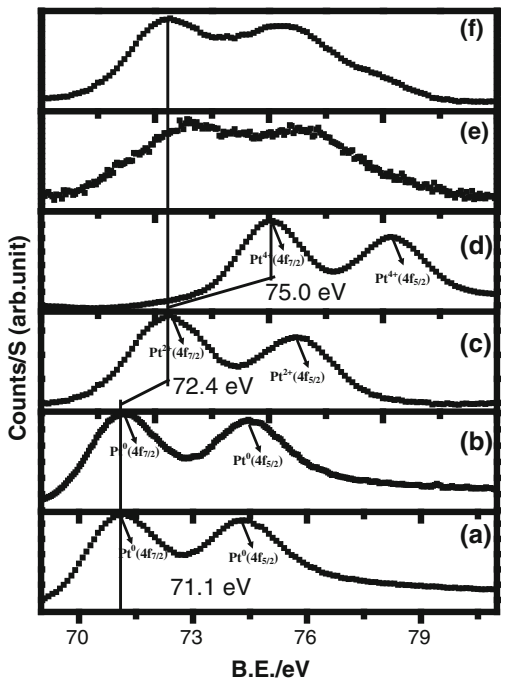

Fig. 3 XPS of Pt(4f) core level in *a* Pt metal foil, *b* 2% Pt/C, *c* $(NH_4)_4Pt(NO_3)_2$, *d* PtO_2, *e* Pt(4f) core level in as prepared $Ce_{0.98}Pt_{0.02}O_{2-\delta}$, and *f* Pt(4f) core level spectrum core level spectrum obtained by the addition of PtO_2 and PtO in the ratio of 75:25

In $Ce_{0.98}Pt_{0.02}O_{2-\delta}$ compound, Pt(4f) peaks are broad, shifted to higher binding energy suggesting Pt in multiple oxidation states (Fig. 3e). Details on the Pt(4f) spectra of this material can be found elsewhere [36–42] where Pt^0 was found at 71.2, Pt^{2+} at 72.4, and Pt^{4+} at 74.4 eV similar to what was observed by Matolín et al. [47]. Here also, $Pt^{2+}(4f)$ and $Pt^{4+}(4f)$ spectra from $Pt(NH_3)_4(NO_3)_2$ and PtO_2, respectively, were added in the different ratios, and one such spectrum having the mixed valent Pt^{2+} and Pt^{4+} in the ratio of 0.75:0.25 is given in Fig. 3f. Pt(4f) spectrum from $Ce_{0.98}Pt_{0.02}O_{2-\delta}$ shown in Fig. 3e gives similar spectrum as given in Fig. 3f concluding that the Pt^{2+} and Pt^{4+} ratio is ~0.75:0.25. Ce(3d) spectrum from $Ce_{0.98}Pt_{0.02}O_{2-\delta}$ shows almost 90% of cerium in 4+ state (not shown) and spectrum looks similar to Fig. 2a. Thus, the composition from Pt and Ce ratios comes out to be $Ce_{0.98}Pt_{0.02}O_{1.95}$ indicating the oxide ion vacancies.

Similarly, from the XPS of Pt(4f) core level spectrum in $Ce_{0.83}Ti_{0.15}Pt_{0.02}O_{2-\delta}$ gives 60% Pt in +2 state and 40% Pt is in +4 state (Fig. 4a). Here also, Ce is found almost in 90% in +4 state (not shown). Ti(2p) core level spectrum

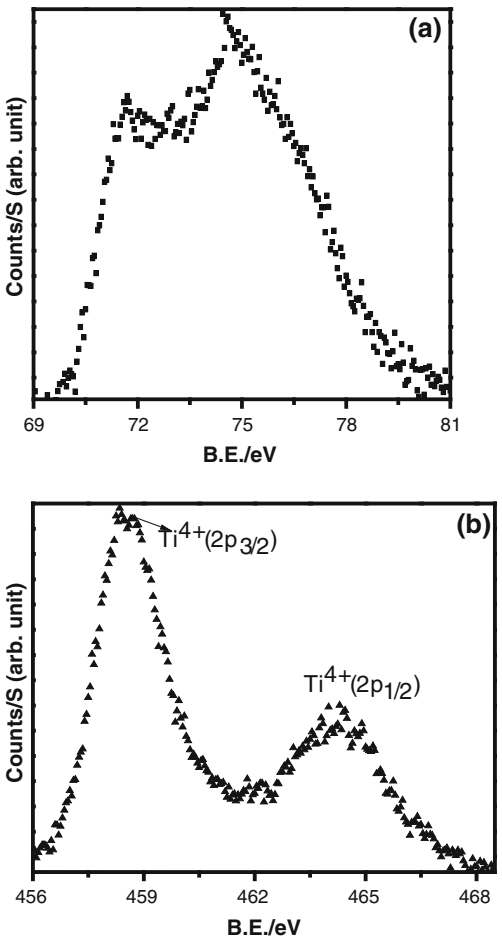

Fig. 4 XPS of **a** Pt(4f) core level and **b** Ti(2p) core level in as prepared $Ce_{0.83}Pt_{0.02}Ti_{0.15}O_{2-\delta}$

gives two peaks at 458.7 and 464.5 eV confirming Ti in +4 state (Fig. 4b).

Redox behavior and oxygen evolution reaction in acid medium

Oxygen evolution in acidic medium occurs with the reaction

$$2H_2O \rightarrow O_2 + 4H^+ + 4e^- \quad (6)$$

This reaction occurs at 1.23 V with respect to standard hydrogen electrode [48]. Cyclic voltammograms (CV) for CeO_2 and $Ce_{1-x}Pt_xO_{2-\delta}$ (x=0.01, 0.015, 0.02) in 0.5 M H_2SO_4 at a scan rate of 5 mV/s are shown in Fig. 5a in the potential range of −0.2 to +1.5 V. Cyclic voltammogram of CeO_2 shows two redox couples: (a) Adsorption of hydroxide coverage and its subsequent reduction appear at 0.56 and 0.36 V, respectively, and (b) oxidation peak at 1.38 V with the subsequent reduction peak at 1.16 is observed due to the Ce^{3+}/Ce^{4+} redox couple in CeO_2. Oxidation and reduction potential values of cerium are in good agreement with the reported values [49, 50]. Presence of Ce^{3+} ion in CeO_2, $Ce_{1-x}Pt_xO_{2-\delta}$, and $Ce_{0.83}Ti_{0.15}Pt_{0.02}O_{2-\delta}$ as seen in the XPS can be further confirmed by their CVs.

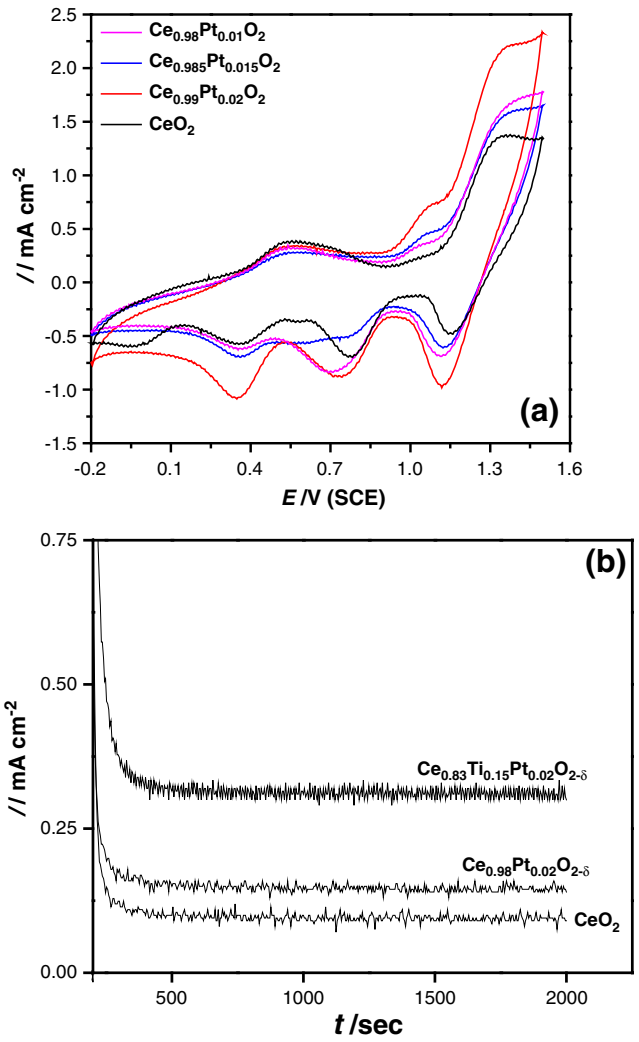

Fig. 5 Cyclic voltammograms in 0.5 M H_2SO_4 for **a** CeO_2 and $Ce_{1-x}Pt_xO_{2-\delta}$ (x=0.01, 0.015, and 0.02) and **b** chronoamperometry at 1.2 V in 0.5 M H_2SO_4 for CeO_2, $Ce_{0.98}Pt_{0.02}O_{2-\delta}$, and $Ce_{0.83}Ti_{0.15}Pt_{0.02}O_{2-\delta}$

Cerium oxidation and reduction was confirmed by performing CV in the aqueous solution of the mixture of Ce^{3+}–Ce^{4+} ions in the solutions of $Ce(NO_3)_3$ and $(NH_4)_2Ce(NO_3)_6$ which gave similar redox couple at almost same potentials. $Ce_{1-x}Pt_xO_{2-\delta}$ decreases the onset potential of oxygen evolution compared with the CeO_2 (Fig. 5a). Oxidation peak of Ce^{3+} to Ce^{4+} lies in the potential range where oxygen evolution starts. Bubbles can be seen on the $Ce_{1-x}Pt_xO_{2-\delta}$ (more prominently on $Ce_{0.98}Pt_{0.02}O_{2-\delta}$) electrode surface above 1.1 V which confirms the oxygen evolution. CeO_2 electrode shows bubbling only after 1.4 V which confirms the catalytic effect of Pt in CeO_2.

To quantify the high current gain observed in CV, chronoamperometry experiment for 1,800 s is carried out for CeO_2, $Ce_{0.98}Pt_{0.02}O_{2-\delta}$, and $Ce_{0.83}Ti_{0.15}Pt_{0.02}O_{2-\delta}$ as shown in Fig. 5b. Steady-state current density values are 0.09, 0.15, and 0.31 mA cm^{-2} for CeO_2, $Ce_{0.98}Pt_{0.02}O_{2-\delta}$, and $Ce_{0.84}Ti_{0.15}Pt_{0.01}O_{2-\delta}$, respectively. In a separate experiment, after a prolonged chronoamperometry experiment, CeO_2 showed almost no current while $Ce_{0.98}Pt_{0.02}O_{2-\delta}$ and $Ce_{0.83}Ti_{0.15}Pt_{0.02}O_{2-\delta}$ did not show any significant decay in the current (not shown). Hence, the latter two compounds reach a steady state after the initial current loss acting as electrocatalysts.

Clearly, Pt ion substitution in CeO_2 or $Ce_{1-x}Ti_xO_2$ improves the electrocatalytic property of oxygen evolution and CeO_2 is not as active as $Ce_{0.98}Pt_{0.02}O_{2-\delta}$ and $Ce_{0.84}Ti_{0.15}Pt_{0.01}O_{2-\delta}$. To understand this behavior, we mapped electronic structure of the electrodes by XPS after the chronoamperometry experiments. Interestingly, CeO_2 shows a substantial (~90%) reduction of Ce^{4+} ion giving Ce^{3+} state (Fig. 6d). For comparison, we have reproduced the Fig. 2 along with it (Fig. 6a–c). It is now easy to understand that Fig. 6d is similar to Fig. 6c which is the core level spectra of Ce^{3+}. Because of the extensive reduction of CeO_2, current decayed during the applied potential of 1.2 V and a very small current is achieved. As positive potential causes the oxidation processes to happen, reduction in CeO_2 should be accompanying with a parallel oxidation reaction causing the reduction in the CeO_2 which can only be the oxidation of the negatively charged oxygen from the CeO_2 lattice that is $O^{2-} \rightarrow O_2 + 2e^-$. As CeO_2 is a reducible oxide so the oxidation of O^{2-} is quite reasonable. An important conclusion which can be drawn from this

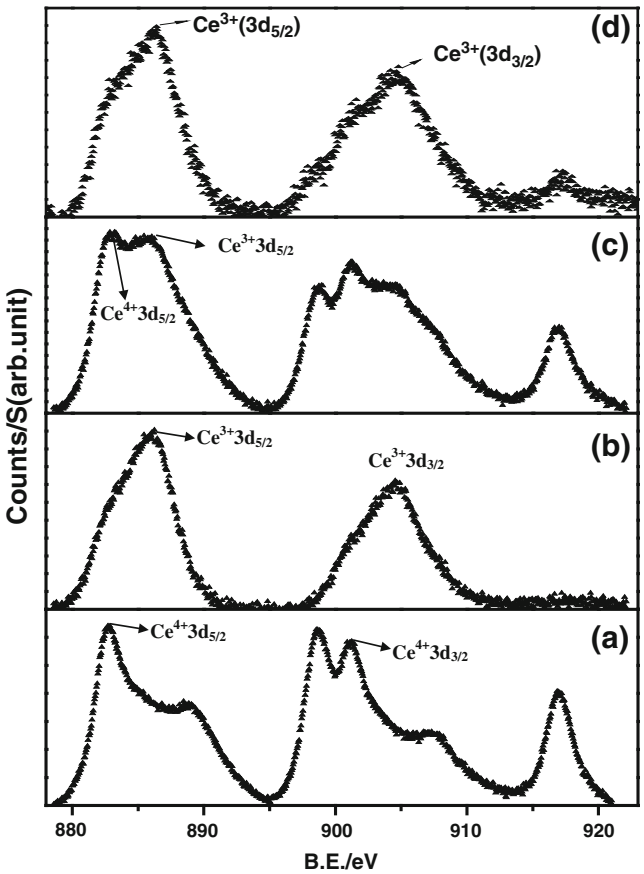

Fig. 6 XPS of Ce(3d) core level spectra in *a* CeO_2, *b* Ce_2O_3, and *c* Ce (3d) core level spectrum obtained by the addition of CeO_2 and Ce_2O_3 in the ratio of 50:50 and **d** Ce(3d) core level region in CeO_2 after putting an electrochemical potential of 1.2 V for 1,800 s in H_2SO_4

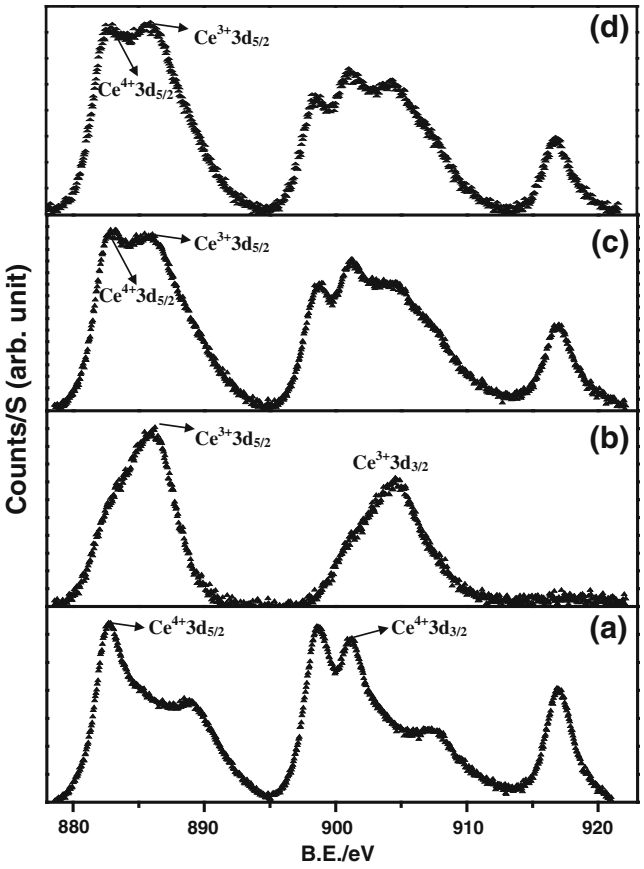

Fig. 7 XPS of Ce(3d) core level spectra in *a* CeO_2, *b* Ce_2O_3, and *c* Ce (3d) core level spectrum obtained by the addition of CeO_2, Ce_2O_3 in the ratio of 50:50 and *d* Ce(3d) core level region in $Ce_{0.98}Pt_{0.02}O_{2-\delta}$ after putting an electrochemical potential of 1.2 V for 1,800 s

observation is that lattice oxygen of CeO_2 can be oxidized under the positive electrochemical potential. On the other hand, in $Ce_{0.98}Pt_{0.02}O_{2-\delta}$, at steady state, platinum is partially oxidized to give more Pt^{4+} compared with the fresh catalyst after chronoamperometry experiment with Pt^{2+}-to-Pt^{4+} ratio equal to 0.60:0.40 (not shown), and Ce^{4+} is reduced to only about 50% (Fig. 7d) which is far lower than the reduction of CeO_2 electrode (compare Fig. 7d with Fig. 6d). For comparison, we have given the Fig. 7a–c which are the reproduction of Fig. 2 for better understanding. Spectra in Fig. 7d resemble to Fig. 7c which has been obtained by mixing 50% of both Ce^{4+} and Ce^{3+} core level XPS spectra. Observation of a finite steady-state current at this stage is thus due to the establishment of equilibrium between Pt^{2+}–Pt^{4+} and Ce^{4+}–Ce^{3+} redox couple. In other words, at the steady state, equilibrium between Pt^{2+}/Pt^{4+}–Ce^{4+}/Ce^{3+} gives rise to the oxygen evolution reaction through the reaction 5. Hence, due to the electronic interaction between Pt^{2+}/Pt^{4+} and Ce^{4+}/Ce^{3+}, $Ce_{0.98}Pt_{0.02}O_{2-\delta}$ works as an electrocatalyst. Similar explanation holds true in the case of $Ce_{0.83}Ti_{0.15}Pt_{0.02}O_{2-\delta}$ also. Platinum in this case also is partially oxidized from Pt^{2+} to Pt^{4+} in the ratio equal to 0.60:0.40 (not shown). More importantly, Ce^{4+} reduction in $Ce_{0.83}Ti_{0.15}Pt_{0.02}O_{2-\delta}$ is only 25% (Fig. 8d) which is much lower than 50% in $Ce_{0.98}Pt_{0.02}O_{2-\delta}$ (compare with Figs. 6d and 7d). For the better understanding Fig. 8a–c is the reproduction of Fig. 2. Clearly Ce^{3+} formation is almost half to that shown in Fig. 8c. Thus, $Ce_{0.83}Ti_{0.15}Pt_{0.02}O_{2-\delta}$ is more stable and hence shows a very less drop in current in chronoamperometry compared with $Ce_{0.98}Pt_{0.02}O_{2-\delta}$ giving rise to higher steady-state current. Hence, observation of much higher oxygen evolution current in $Ce_{0.83}Ti_{0.15}Pt_{0.02}O_{2-\delta}$ compared with $Ce_{0.98}Pt_{0.02}O_{2-\delta}$ (see Fig. 5b) is due to more stable nature of CeO_2 in the former catalyst. Hence, Pt ion substitution plays a role behind the chemistry of lattice oxygen of CeO_2. There was no clear indication of Ti^{4+} ion reduction as evidenced from Ti(2p) core level spectrum due to applied potential of 1.2 V for 1,800 s (not shown). Percentage reduction of Ce^{4+} estimated from the XPS is 90%, 50%, and 25 % for CeO_2, $Ce_{0.98}Pt_{0.02}O_{2-\delta}$, and $Ce_{0.83}Ti_{0.15}Pt_{0.02}O_{2-\delta}$, respectively.

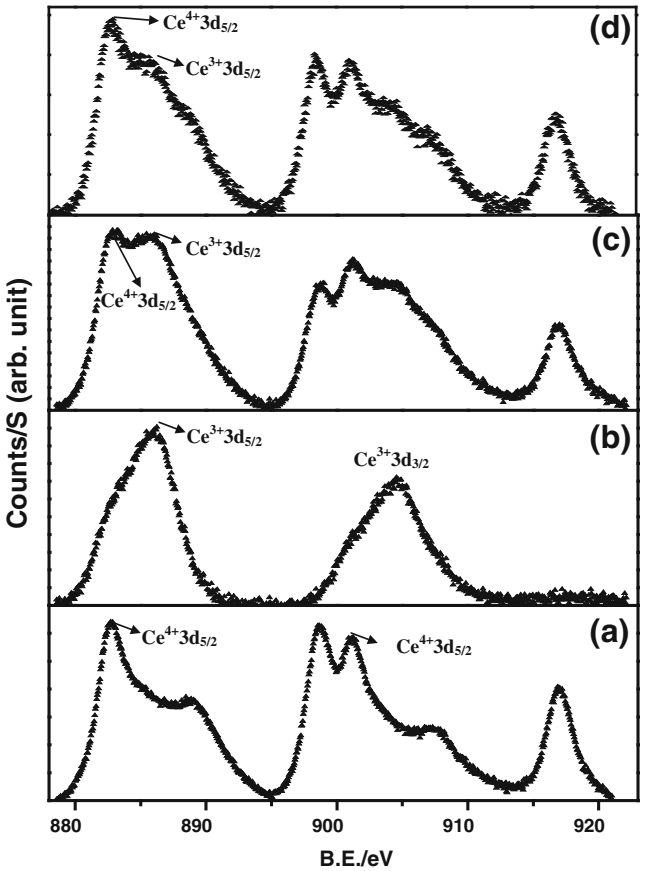

Fig. 8 XPS of Ce(3d) core level spectra in *a* CeO_2, *b* Ce_2O_3, and *c* Ce (3d) core level spectrum obtained by the addition of CeO_2 and Ce_2O_3 in the ratio of 50:50 and *d* Ce(3d) core level region in $Ce_{0.83}Ti_{0.15}Pt_{0.02}O_{2-\delta}$ after putting an electrochemical potential of 1.2 V for 1,800 s

Based on above experimental observations redox behavior of CeO_2 in aqueous acidic solution at 1.2 V can be written as follows:

$$CeO_2 + H_2O \rightarrow Ce^{4+}{}_{1-z}Ce^{3+}{}_zO_{2-z/2} + 2H^+ + 2\overline{e} + 1/2(1+z/2)\,O_2 (z \sim 0.9) \quad (7)$$

Once CeO_2 is reduced to $CeO_{1.55}$, there is little electrocatalytic activity.

Oxygen evolution over $Ce_{1-x}Pt_xO_{2-\delta}$ at 1.2 V can be written as follows:

$$Ce_{1-x}Pt_xO_{2-\delta} + H_2O \Leftrightarrow Ce_{1-x}Pt_xO_{2-\delta-z/2} + 2H^+ + 2\overline{e} + 1/2(1+z/2)O_2 (x \sim 0.02, z \sim 0.5) \quad (8)$$

Once the steady state with z=0.5 is reached, further reaction is due to the water splitting $[2H_2O \rightarrow O_2 + 4H^+ + 4e^- \ldots (5)]$.

Similarly, at 1.2 V potential, oxygen evolution over $Ce_{1-x-y}Ti_xPt_yO_{2-\delta}$ can be written as follows:

$$Ce_{1-x-y}Ti_xPt_yO_{2-\delta} + H_2O \Leftrightarrow Ce_{1-x-y}Ti_xPt_yO_{2-\delta-z} + 2H^+ + 2\overline{e} + 1/2\,(1+z/2)\,O_2\ (x = 0.02,\ y = 0.15z \sim 0.25) \quad (9)$$

Here also, once the steady state is reached at z=0.25, reaction 5 takes over. Notice that the O_2 evolution is very low for CeO_2 from reaction 5 compared with $Ce_{0.98}Pt_{0.02}O_{2-\delta}$ and $Ce_{0.84}Ti_{0.15}Pt_{0.01}O_{2-\delta}$.

Thus, mapping the electrode composition by XPS after chronoamperometry experiments, one can conclude that steady-state current in oxygen evolution is directly related to extent of Ce^{4+} ion reduction and hence the stability of CeO_2. The lower the Ce^{4+} ion reduction, the higher the oxygen evolution current. Pt ions in CeO_2 and in $Ce_{0.85}Ti_{0.15}O_{2-\delta}$ control the lattice oxygen in a particular way to impart the activity in CeO_2 and $Ce_{0.85}Ti_{0.15}O_{2-\delta}$. Although only positive potential is applied in both the processes, reduction in both $Ce_{0.98}Pt_{0.02}O_{2-\delta}$ and $Ce_{0.83}Ti_{0.15}Pt_{0.02}O_{2-\delta}$ signifies the oxidation of O^{2-} to $1/2O_2$ which promptly raises a question if this lattice oxygen can be utilized to remove the CO poisoning effect arises in the electrooxidation of formic acid and methanol? So, in the following section, we will demonstrate the activity of $Ce_{0.98}Pt_{0.02}O_{2-\delta}$ and $Ce_{0.84}Ti_{0.15}Pt_{0.01}O_{2-\delta}$ for formic acid and methanol electrooxidation and compare with Pt/C catalyst consisting of the same amount of platinum.

Formic acid electrooxidation

Cyclic voltammograms in the solution of 0.5 M HCOOH and 0.5 M H_2SO_4 in the potential range of 0.0–1.0 V for $Ce_{0.98}Pt_{0.02}O_{2-\delta}$, $Ce_{0.83}Ti_{0.15}Pt_{0.02}O_{2-\delta}$, and 2% Pt/C are given in Fig. 9a. Amount of Pt is same (22.4 mg/g) in each of the electrodes. Notice almost no current with 2% Pt/C electrode. However, 5% Pt/C did show a little current corresponding to formic acid oxidation (Fig. 9b). Due to CO poisoning in 5% Pt/C, a very low current is observed in the anodic sweep, but in the reverse scan, noticeable current is observed corresponding to formic acid oxidation (indicated by vertical arrow). Against this, in anodic sweep, a huge current density corresponding to formic acid oxidation over $Ce_{0.98}Pt_{0.02}O_{2-\delta}$ and $Ce_{0.84}Pt_{0.02}Ti_{0.15}O_{2-\delta}$ is attained with an onset potential of 0.4 V. Maximum activity is attained at ~0.7 V with both $Ce_{0.98}Pt_{0.02}O_{2-\delta}$ and $Ce_{0.84}Ti_{0.15}Pt_{0.01}O_{2-\delta}$. In the reverse sweep, we do not see any peak indicating that there is no CO poisoning over these two electrodes. Rate of forward reaction will be lower than the rate of backward reaction if there is CO formation on the electrode. Further, in cyclic voltammetry, both

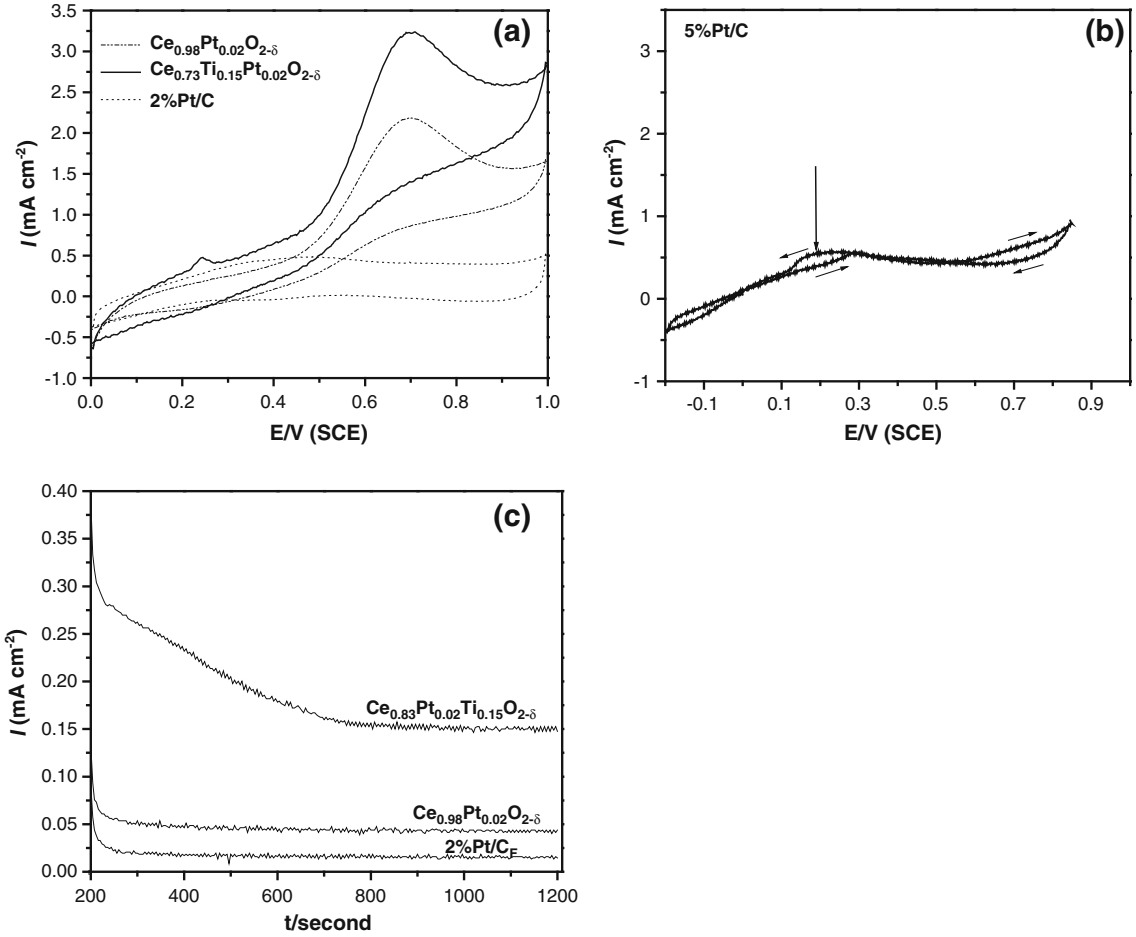

Fig. 9 Cyclic voltammogram of **a** 2% Pt/C, $Ce_{0.98}Pt_{0.02}O_{2-\delta}$ and $Ce_{0.84}Pt_{0.02}Ti_{0.15}O_{2-\delta}$ and **b** 5% Pt/C and chronoamperometry **c** at 0.7 V in for 2% Pt/C, $Ce_{0.98}Pt_{0.02}O_{2-\delta}$, and $Ce_{0.83}Ti_{0.15}Pt_{0.02}O_{2-\delta}$ in 0.5 M H_2SO_4+0.5 M HCOOH

$Ce_{0.98}Pt_{0.02}O_{2-\delta}$ and $Ce_{0.83}Ti_{0.15}Pt_{0.02}O_{2-\delta}$ show a continuous rise till a maxima appears at 1.0 V which again indicates the absence of any poisoning due to CO which would have resulted in a very small peak in the forward scan [21, 22]. Thus, ionic Pt in $Ce_{0.98}Pt_{0.02}O_{2-\delta}$ and $Ce_{0.83}Ti_{0.15}Pt_{0.02}O_{2-\delta}$ indeed eliminates CO poisoning effect.

Having observed enhanced electrocatalytic activity with $Ce_{0.98}Pt_{0.02}O_{2-\delta}$ and $Ce_{0.83}Ti_{0.15}Pt_{0.02}O_{2-\delta}$ catalyst in the CV, chronoamperometry experiments are carried out. In Fig. 9c, we show an amperogram at 0.7 V for $Ce_{0.98}Pt_{0.02}O_{2-\delta}$, $Ce_{0.84}Pt_{0.02}Ti_{0.15}O_{2-\delta}$, and 2% Pt/C. Current gain is 0.15 for $Ce_{0.98}Pt_{0.02}O_{2-\delta}$, 0.43 for $Ce_{0.83}Ti_{0.15}Pt_{0.02}O_{2-\delta}$, and 0.014 for 2% Pt/C, respectively. Clearly, $Ce_{0.84}Pt_{0.02}Ti_{0.15}O_{2-\delta}$ shows ten times higher activity compared with 2% Pt/C with the same amount of Pt in each of the electrode.

To understand what makes $Ce_{0.98}Pt_{0.02}O_{2-\delta}$ and $Ce_{0.84}Pt_{0.02}Ti_{0.15}O_{2-\delta}$ to remove the CO poisoning effect and enhancing the electrocatalytic activity compared with 2% Pt/C toward the electrooxidation of formic acid, XPS mapping of the surface of the electrodes after CV and chronoamperometric experiments in the solution of 0.5 M HCOOH and 0.5 M H_2SO_4 was carried out. Pt^{2+}/Pt^{4+} states remain almost unchanged after the CV as well as chronoamperometry in the formic acid solution for both $Ce_{0.98}Pt_{0.02}O_{2-\delta}$ and $Ce_{0.84}Pt_{0.02}Ti_{0.15}O_{2-\delta}$ electrodes. Ce (3d) core level spectrum in $Ce_{0.98}Pt_{0.02}O_{2-\delta}$ after cycling is showing the extent of Ce^{4+} reduction almost 50% (not shown) and spectrum looks similar to Fig. 7d. Almost similar extent of Ce^{4+} reduction is noticed after chronoamperometry experiment also. Extent of Ce^{4+} reduction in $Ce_{0.84}Pt_{0.02}Ti_{0.15}O_{2-\delta}$ is only about 25% after CV as well as after chronoamperometry experiments (not shown). Spectra thus obtained similar look as shown in Fig. 8d. Hence, Ce^{4+} is still the major component in $Ce_{0.83}Ti_{0.15}Pt_{0.02}O_{2-\delta}$ after electrochemical treatment in the formic acid solution. Ti (2p) core level spectra do not show any significant change after the cyclic voltammetry as well as after chronoamperometry experiments (not shown).

Reduction of Ce^{4+} in $Ce_{0.98}Pt_{0.02}O_{2-\delta}$ as well as in $Ce_{0.83}Ti_{0.15}Pt_{0.02}O_{2-\delta}$ after chronoamperometry and cyclic

voltammetry indicate that lattice oxygen is utilized initially and steady state is reached with an equilibrium concentration of Pt^{2+}/Pt^{4+}–Ce^{4+}/Ce^{3+} states. It has been stated earlier and should be emphasized again that when a positive potential is applied, reduction in both $Ce_{0.98}Pt_{0.02}O_{2-\delta}$ and $Ce_{0.83}Ti_{0.15}Pt_{0.02}O_{2-\delta}$ signifies the oxidation of O^{2-} to $1/2O_2$ causing the reduction of the catalytic surface. This indicates that the removal of CO poisoning in the lower potential range is due to the involvement of lattice oxygen. CO adsorbed over the catalyst surface according to reaction 2 makes use of lattice oxygen to give CO_2 and thus CO poisoning is eliminated. Based on above observations, formic acid electro-oxidation over $Ce_{0.98}Pt_{0.02}O_{2-\delta}$ surface can be written as:

$$Ce_{1-x}Pt_xO_{2-\delta} + y\,HCOOH \rightarrow {Ce^{4+}}_{1-x-2y}{Ce^{3+}}_{2y}Pt_xO_{2-\delta} + yH_2O + yCO_2 (y \sim 0.25) \quad (10)$$

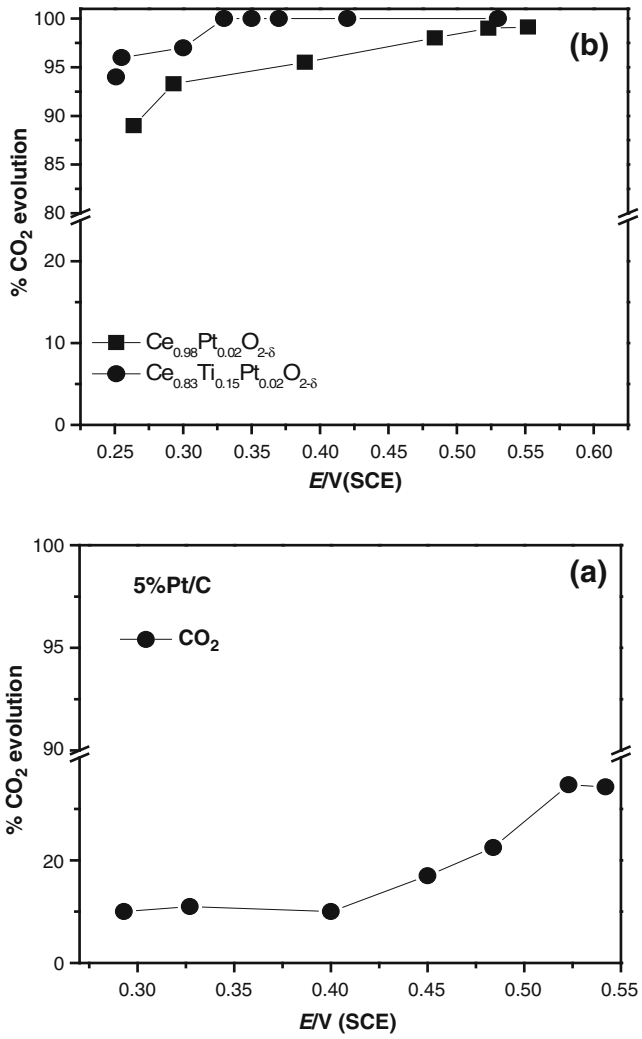

Fig. 10 Percent CO_2 formation in the output gases from the cell at different potentials for **a** 5% Pt/C and **b** $Ce_{0.99}Pt_{0.01}O_{2-\delta}$ and $Ce_{0.83}Ti_{0.15}Pt_{0.02}O_{2-\delta}$ in 0.5 M H_2SO_4+0.5 M HCOOH

Small changes occurring in Pt oxidation state are neglected for the sake of simplicity

$$HCOOH \rightarrow CO_2 + 2H^+ + 2\bar{e} \quad (11)$$

Once the steady state equilibrium composition is reached on ~500 s according to reaction 10, reaction 11 seems to take over leading to formic acid oxidation via pathway 1. Initial current loss due to Ce^{4+} reduction is more in the case of $Ce_{0.98}Pt_{0.02}O_{2-\delta}$ compared with $Ce_{0.83}Ti_{0.15}Pt_{0.02}O_{2-\delta}$ resulting in lower steady-state current. Further, after the CV experiment, cerium reduction is more in $Ce_{0.98}Pt_{0.02}O_{2-\delta}$ compared with $Ce_{0.83}Ti_{0.15}Pt_{0.02}O_{2-\delta}$ indicating that $Ce_{0.83}Ti_{0.15}Pt_{0.02}O_{2-\delta}$ is more stable than $Ce_{0.98}Pt_{0.02}O_{2-\delta}$. Pt state in both the compounds is almost unaffected before and after the experiments. Ti is also stable in +4 state in $Ce_{0.84}Ti_{0.15}Pt_{0.01}O_{2-\delta}$. This confirms that $Ce_{0.83}Ti_{0.15}Pt_{0.02}O_{2-\delta}$ reaches a more stable composition and hence a better electrocatalyst compared with $Ce_{0.98}Pt_{0.02}O_{2-\delta}$.

Analysis of output gases during HCOOH oxidation

Enhancement in formic acid oxidation by Pt ions in $Ce_{0.98}Pt_{0.02}O_{2-\delta}$ and $Ce_{0.84}Pt_{0.02}Ti_{0.15}O_{2-\delta}$ compared with Pt^0 in 2% Pt/C has been confirmed by analyzing the CO_2 gases evolved by an online gas chromatograph as a function

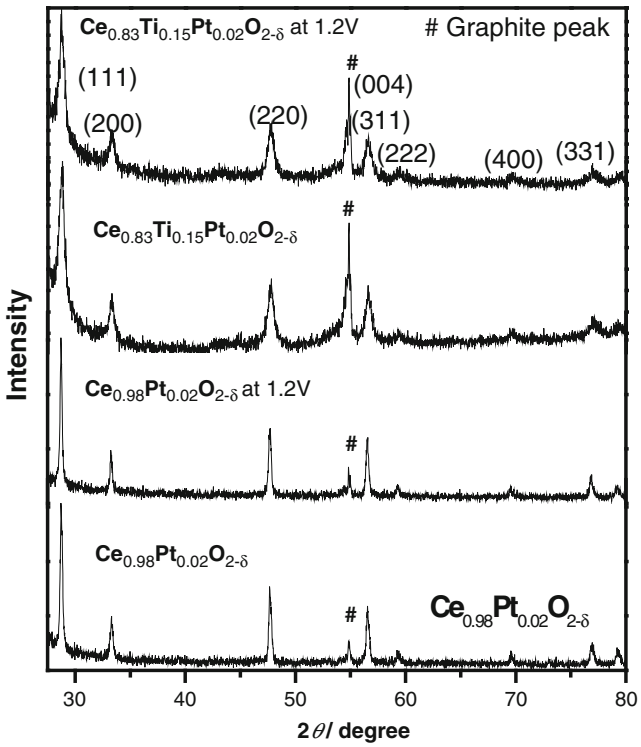

Fig. 11 XRD patterns for $Ce_{0.98}Pt_{0.02}O_{2-\delta}$ in fresh electrode, $Ce_{0.98}Pt_{0.02}O_{2-\delta}$ after chronoamperometry for 1,000 s in 0.5 M H_2SO_4+0.5 M HCOOH, $Ce_{0.83}Ti_{0.15}Pt_{0.02}O_{2-\delta}$ in fresh electrode and $Ce_{0.83}Ti_{0.15}Pt_{0.02}O_{2-\delta}$ after chronoamperometry for 1,000 s in 0.5 M H_2SO_4+0.5 M HCOOH

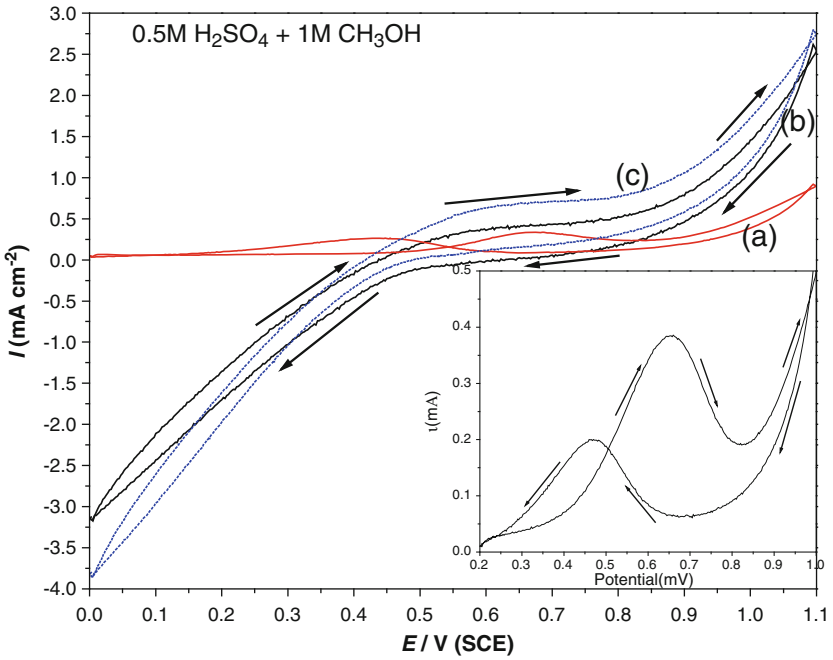

Fig. 12 Cyclic voltammogram of for methanol oxidation with *a* 2% Pt/C, *b* $Ce_{0.98}Pt_{0.02}O_{2-\delta}$, and *c* $Ce_{0.83}Ti_{0.15}Pt_{0.02}O_{2-\delta}$. Enlarge plot methanol oxidation with 2% Pt/C is given in *inset* for better clarity

of potential. CO_2 evolution over 2% Pt/C was too low to be detected, and also, it gets polarized easily during formic acid oxidation. Hence, experiment is done with 5% Pt/C. CO_2 formation with 5% Pt/C, $Ce_{0.98}Pt_{0.02}O_{2-\delta}$ and $Ce_{0.84}Pt_{0.02}Ti_{0.15}O_{2-\delta}$, as a function of applied potential is shown in a and b of Fig. 10, respectively. With 5% Pt/C, maximum CO_2 formation is 52% at potential higher than 0.48 V. At 0.40 V and below CO_2 formation is only 10%. Against this, $Ce_{0.99}Pt_{0.01}O_{2-\delta}$ gives ~100% CO_2 formation at potentials 0.45 V and onwards. Even in the lower potential range, 0.25 to 0.45 CO_2 formation is in the range of 90–95% which is quite higher than 5% Pt/C. Remarkably, $Ce_{0.83}Ti_{0.15}Pt_{0.02}O_{2-\delta}$ shows 100% CO_2 formation even at 0.35 V. The analysis is done up to 1.0 V and CO_2 formation remains constant at 100% over Pt^{2+} ions substituted oxides. Thus, ionic Pt dispersed in CeO_2 and $Ce_{1-x}Ti_xO_2$ in the form of solid solution $Ce_{1-x}Pt_xO_{2-\delta}$ and $Ce_{1-x-y}Ti_yPt_xO_{2-\delta}$ indeed eliminates CO poisoning effect for HCOOH oxidation. Higher amount of CO_2 at lower potential indicates the catalytic effect of Pt^{2+} ions in CeO_2 and $Ce_{1-x}Ti_xO_2$ compared with Pt in C.

XRD patterns before and after the chronoamperometry in the solution of 0.5 M HCOOH and 0.5 M H_2SO_4 for both $Ce_{0.98}Pt_{0.02}O_{2-\delta}$ and $Ce_{0.84}Pt_{0.02}Ti_{0.15}O_{2-\delta}$ do not show any change as shown in Fig. 11. This means that there are no changes in the fluorite structure of both the electrodes after the electrochemical experiments.

Methanol oxidation

After studying the oxygen evolution and formic acid oxidation, catalysts were tested for methanol oxidation in acidic medium. Cyclic voltammogram for the methanol oxidation in the solution of 1.0 M methanol+0.5 M H_2SO_4 with 2% Pt/C, $Ce_{0.98}Pt_{0.02}O_{2-\delta}$, and $Ce_{0.83}Ti_{0.15}Pt_{0.02}O_{2-\delta}$ are shown in a–c of Fig. 12, respectively. Methanol

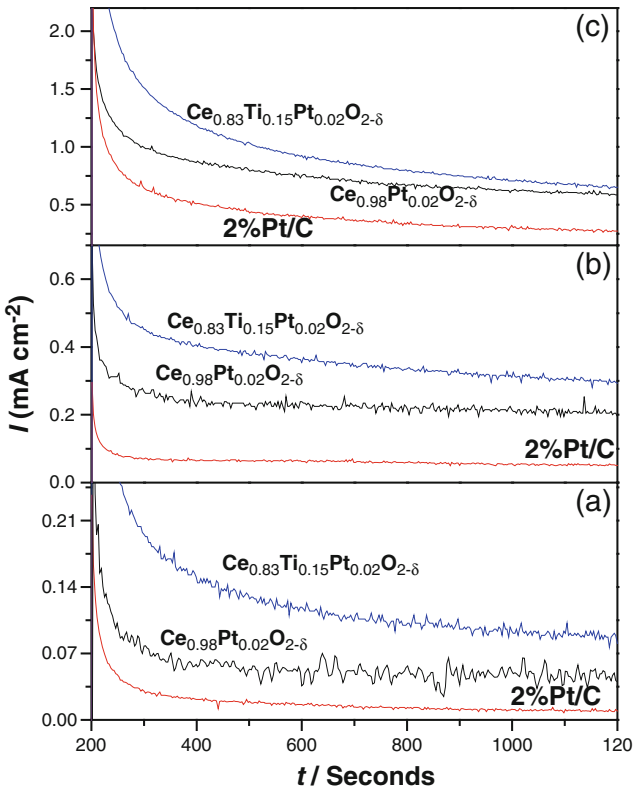

Fig. 13 Chronoamperometry in methanol oxidation with 2% Pt/C (*red line*), $Ce_{0.98}Pt_{0.02}O_{2-\delta}$ (*black line*), and $Ce_{0.83}Ti_{0.15}Pt_{0.02}O_{2-\delta}$ (*blue line*) at 0.65, 0.9, and 1.1 V in *a*, *b*, and *c*, respectively

oxidation plot with 2% Pt/C in the range of 0.2–1.0 V is also shown in inset of Fig. 12 for better visibility. Pt^{2+} ion in CeO_2 and $Ce_{0.85}Ti_{0.15}O_2$ has shown higher activity compared with Pt metal in 2% Pt/C. Higher activity of these catalysts was further investigated by chronoamperometry at 0.65, 0.9, and 1.1 V as shown in a–c of Fig. 13, respectively. With the same amount of Pt, $Ce_{0.98}Pt_{0.02}O_{2-\delta}$ shows five times and $Ce_{0.83}Ti_{0.15}Pt_{0.02}O_{2-\delta}$ shows 10 times higher activity than 2% Pt/C. At higher potential also, approximately three to five times higher activity was observed with $Ce_{0.98}Pt_{0.02}O_{2-\delta}$ and $Ce_{0.83}Ti_{0.15}Pt_{0.02}O_{2-\delta}$

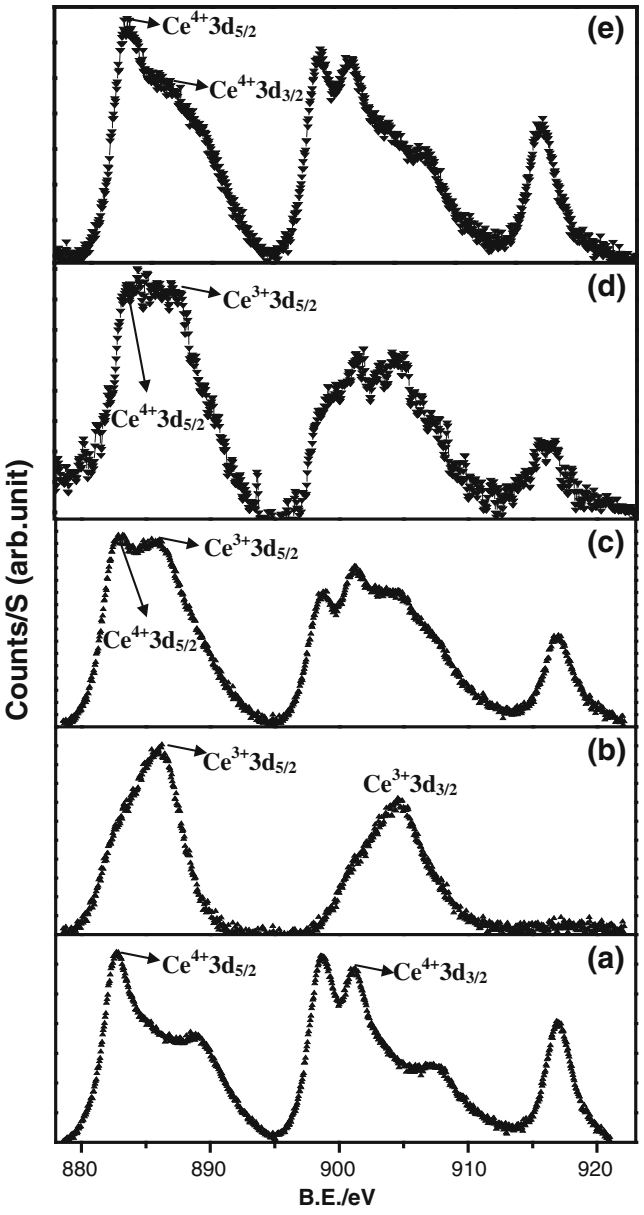

Fig. 14 XPS of Ce(3d) core level spectra in *a* CeO_2, *b* Ce_2O_3, and *c* Ce(3d) core level spectrum obtained by the addition of CeO_2 and Ce_2O_3 in the ratio of 50:50. Ce(3d) core level spectra after cyclic voltammetry experiment up to 1.1 V for methanol oxidation in *d* $Ce_{0.98}Pt_{0.02}O_{2-\delta}$ and *e* $Ce_{0.83}Ti_{0.15}Pt_{0.02}O_{2-\delta}$

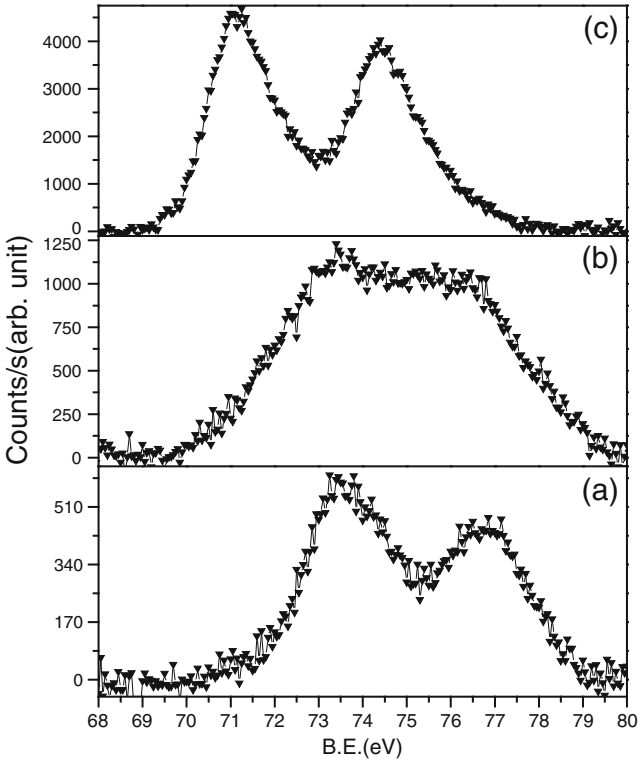

Fig. 15 XPS of Pt(4f) core level after cyclic voltammetry experiment up to 1.1 V for methanol oxidation *a* $Ce_{0.98}Pt_{0.02}O_{2-\delta}$, *b* $Ce_{0.83}Ti_{0.15}Pt_{0.02}O_{2-\delta}$, and *c* 2% Pt/C, respectively

as compared with 2% Pt/C. After cyclic voltammetry, experiment at 1.1 V XPS of the catalyst was recorded. In the case of $Ce_{0.98}Pt_{0.02}O_{2-\delta}$, Ce(3d) spectra are shown in Fig. 14d and about 55% of cerium is found in +3 state and remaining in 4+ state which is almost the same as observed in Fig. 7d. Here too, Fig. 14a–c is the reproduction of Fig. 2 for better understanding. After the similar experimental

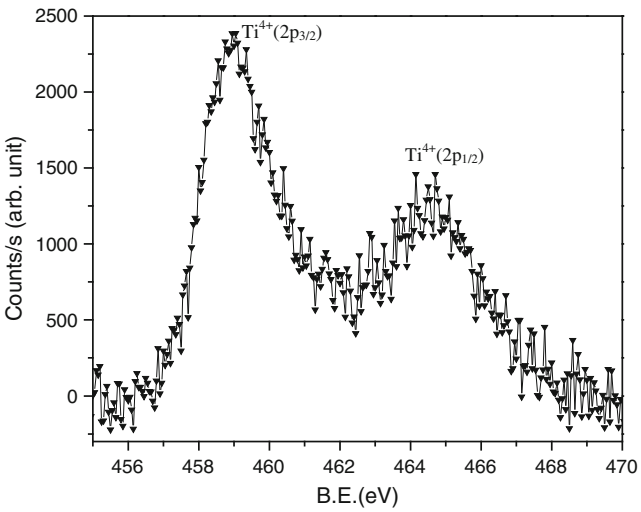

Fig. 16 XPS of Ti(2p) core level in $Ce_{0.83}Ti_{0.15}Pt_{0.02}O_{2-\delta}$ after cyclic voltammetry experiment of methanol oxidation up to 1.1 V

conditions, XPS of Pt(4f) in $Ce_{0.98}Pt_{0.02}O_{2-\delta}$ shows Pt to slightly higher oxidation state resulting in the original binding energy 73 eV (in Fig. 3e) to increase to 73.5 (Fig. 15a). This might be due to the various changes occurring on the surface after applying the positive potential. For example, Pt oxidation state may have changed and/or some local surface changes causing the increase in the binding energy. Similar explanation holds true for Pt in $Ce_{0.83}Ti_{0.15}Pt_{0.02}O_{2-\delta}$. XPS spectra of Ce (3d) in $Ce_{0.83}Ti_{0.15}Pt_{0.02}O_{2-\delta}$ is shown in Fig. 14e, and ~75% of cerium is present in 4+ and the rest is present in 3+ state. Pt(4f) core level spectra for 2% Pt/C show Pt in zero-valent state after cyclic voltammetry experiment. Ti(2p) core XPS from $Ce_{0.83}Ti_{0.15}Pt_{0.02}O_{2-\delta}$ is shown in Fig. 16. Ti still remains in 4+ states only. The presence of higher amount of cerium in 4+ state and Ti in 4+ state in $Ce_{0.83}Ti_{0.15}Pt_{0.02}O_{2-\delta}$ is the reason for high activity of $Ce_{0.83}Ti_{0.15}Pt_{0.02}O_{2-\delta}$ compared with $Ce_{0.98}Pt_{0.02}O_{2-\delta}$ as higher amount of reversible oxygen exchange occurs with $Ce_{0.83}Ti_{0.15}Pt_{0.02}O_{2-\delta}$ lattice compared with $Ce_{0.98}Pt_{0.02}O_{2-\delta}$ lattice. In our earlier work, we have shown that the high reducibility or higher reversible oxygen exchange form lattice is possible with $Ce_{1-x}Ti_xO_2$ compared with CeO_2 [43, 51]. So reaction can be written as

$$Ce_{0.85}Ti_{0.85}Pt_xO_{2-\delta} + yCH_3OH \rightarrow {Ce^{4+}}_{0.85-x-6y}{Ce^{3+}}_{6y}Ti_{0.15}Pt_xO_{2-\delta} + 2yH_2O + yCO_2 \quad (12)$$

$${Ce^{4+}}_{0.85-x-3y}{Ce^{3+}}_{3y}Ti_{0.15}Pt_xO_{2-\delta+}3yH_2O \rightarrow Ce_{0.85}Ti_{0.85}Pt_xO_{2-\delta} + 3yH_2 \quad (13)$$

In conclusion, we have shown that Pt^{2+} ions in CeO_2 and $Ce_{0.85}Ti_{0.15}O_2$ can work as electrocatalysts. Pt^{2+} in CeO_2 and $Ce_{0.85}Ti_{0.15}O_2$ have been shown to have higher activity compared with 2% Pt/C toward oxygen evolution, formic acid oxidation, and methanol oxidation. Activated lattice oxygen in Pt^{2+} ion substituted CeO_2 and $Ce_{0.85}Ti_{0.15}O_2$ have been shown to take active part in oxidation process; hence, higher activity has been observed compared with 2% Pt/C. More importantly, lattice oxygen certainly has a key role in removing the CO poisoning effect.

Acknowledgments The authors thank the Department of Science and Technology for financial support.

References

1. Liu Z, Hong L, Tham MP, Lim TH, Jiang H (2006) J Power Sources 161(2):831–835
2. Jayashree RS, Spendelow JS, Yeom J, Rastogi C, Shannon MA, Kenis PJA (2005) Electrochim Acta 50(24):4674–4682
3. Mrozek MF, Luo H, Weaver MJ (2000) Langmuir 16(22):8463–8469
4. Seland F, Tunold R, Harrington DA (2008) Electrochim Acta 53 (23):6851–6864
5. Hall SC, Subramanian V, Teeter G, Rambabu B (2004) Solid State Ionics 175(1–4):809–813
6. Hall SB, Khudaish EA, Hart AL (1998) Electrochim Acta 43(14–15):2015–2024
7. Walton DJ, Burke LD, Murphy MM (1996) Electrochim Acta 41 (17):2747–2751
8. Willsau J, Wolter O, Heitbaum J (1985) J Electroanal Chem 195 (2):299–306
9. Bockris JOM, Huq AKMS (1956) Proc R Soc Lond Ser A Math Phys Sci (1934–1990) 237(1209):277–296
10. Bera P, Hegde MS, Patil KC (2001) Curr Sci 80:1576–1578
11. Hariprakash B, Bera P, Gaffoor SA, Hegde MS, Shukla AK (2001) J Electrochem Solid State Let 4:A23–A26
12. Jeong K-J, Miesse CM, Choi J-H, Lee J, Han J, Yoon SP, Nam SW, Lim T-H, Lee TG (2007) J Power Sources 168(1):119–125
13. Rice C, Ha S, Masel RI, Wieckowski A (2003) J Power Sources 115(2):229–235
14. Samjeske G, Miki A, Ye S, Osawa M (2006) J Phys Chem B 110 (33):16559–16566
15. Chen YX, Heinen M, Jusys Z, Behm RJ (2006) Angew Chem Int Ed 45(6):981–985
16. Park S, Xie Y, Weaver MJ (2002) Langmuir 18(15):5792–5798
17. Li H, Sun G, Jiang Q, Zhu M, Sun S, Xin Q (2007) Electrochem Comm 9(6):1410–1415
18. Lovic JD, Tripkovic AV, Gojkovic SL, Popovic KD, Tripkovic DV, Olszewski P, Kowal A (2005) J Electroanal Chem 581 (2):294–302
19. Lu G-Q, Crown A, Wieckowski A (1999) J Phys Chem B 103 (44):9700–9711
20. Liu B, Li HY, Die L, Zhang XH, Fan Z, Chen JH (2009) J Power Sources 186(1):62–66
21. Chen W, Kim J, Sun S, Chen S (2007) Langmuir 23(22):11303–11310
22. Choi J-H, Jeong K-J, Dong Y, Han J, Lim T-H, Lee J-S, Sung Y-E (2006) J Power Sources 163(1):71–75
23. Hartung T, Willsau J, Heitbaum J (1986) J Electroanal Chem 205 (1–2):135–149
24. Kang S, Lee J, Lee JK, Chung S-Y, Tak Y (2006) J Phys Chem B 110(14):7270–7274
25. Kim B-J, Kwon K, Rhee CK, Han J, Lim T-H (2008) Electrochim Acta 53(26):7744–7750
26. Wang S, Kristian N, Jiang S, Wang X (2008) Electrochem Comm 10(7):961–964
27. Hoshi N, Kida K, Nakamura M, Nakada M, Osada K (2006) J Phys Chem B 110(25):12480–12484
28. Ha S, Larsen R, Masel RI (2005) J Power Sources 144(1):28–34
29. Huang Y, Zhou X, Liao J, Liu C, Lu T, Xing W (2008) Electrochem Comm 10(4):621–624
30. Larsen R, Ha S, Zakzeski J, Masel RI (2006) J Power Sources 157 (1):78–84
31. Wang R, Liao S, Ji S (2008) J Power Sources 180(1):205–208
32. Yang S, Zhang X, Mi H, Ye X (2008) J Power Sources 175(1):26–32
33. Zhou W, Lee JY (2008) J Phys Chem C 112(10):3789–3793
34. Zhu Y, Kang Y, Zou Z, Zhou Q, Zheng J, Xia B, Yang H (2008) Electrochem Comm 10(5):802–805
35. Persson K, Ersson A, Jansson K, Iverlund N, Järås S (2005) J Catal 231(1):139–150
36. Bera P, Patil KC, Jayaram V, Subbanna GN, Hegde MS (2000) J Catal 196:293
37. Bera P, Gayen A, Hegde MS, Lalla NP, Spadaro L, Frusteri F, Arena F (2003) J Phys Chem B 107(25):6122–6130
38. Kim KS, Winograd N, Davis RE (1971) J Am Chem Soc 93 (23):6296–6297

39. Fachini EoR, Cabrera CR (1999) Langmuir 15:717–721
40. Casella IG, Gatta M (2000) Anal Chem 72:2969–2975
41. Sharma S, Hegde MS (2009) J Chem Phys 130(11):114706–114708
42. Bera P, Priolkar KR, Gayen A, Sarode PR, Hegde MS, Emura S, Kumashiro R, Jayaram V, Subbanna GN (2003) Chem Mater 15 (10):2049–2060
43. Baidya T, Gayen A, Hegde MS, Ravishankar N, Dupont L (2006) J Phys Chem B 110(11):5262–5272
44. Baidya T, Marimuthu A, Hegde MS, Ravishankar N, Madras G (2007) J Phys Chem C 111(2):830–839
45. Kotani A, Ogasawarab H (1992) J Electron Spectrosc Relat Phenom 60:257
46. Murugan B, Ramaswamy AV (2007) J Am Chem Soc 129 (11):3062–3063
47. Matolín V, Matolínova I, Václavú M, Khalakhan I, Vorokhta M, Fiala R, Pis I, Sofer Z, Poltierova-Vejpravova J, Mori T, Potin V, Yoshikawa H, Ueda S, Kobayashi K et al (2010) Langmuir 26 (15):12824–12831
48. Huheey JE, Keiter EA, Keiter RL (2004) Inorganic chemistry. Pearson Education, Upper Saddle River
49. Been J, Oloman CW (1993) J Appl Electrochem 23(12):1301–1309
50. Bishop E, Cofre P (1981) Analyst 106:316–322
51. Dutta G, Waghmare UV, Baidya T, Hegde MS, Priolkar KR, Sarode PR (2006) Chem Mater 18:3249